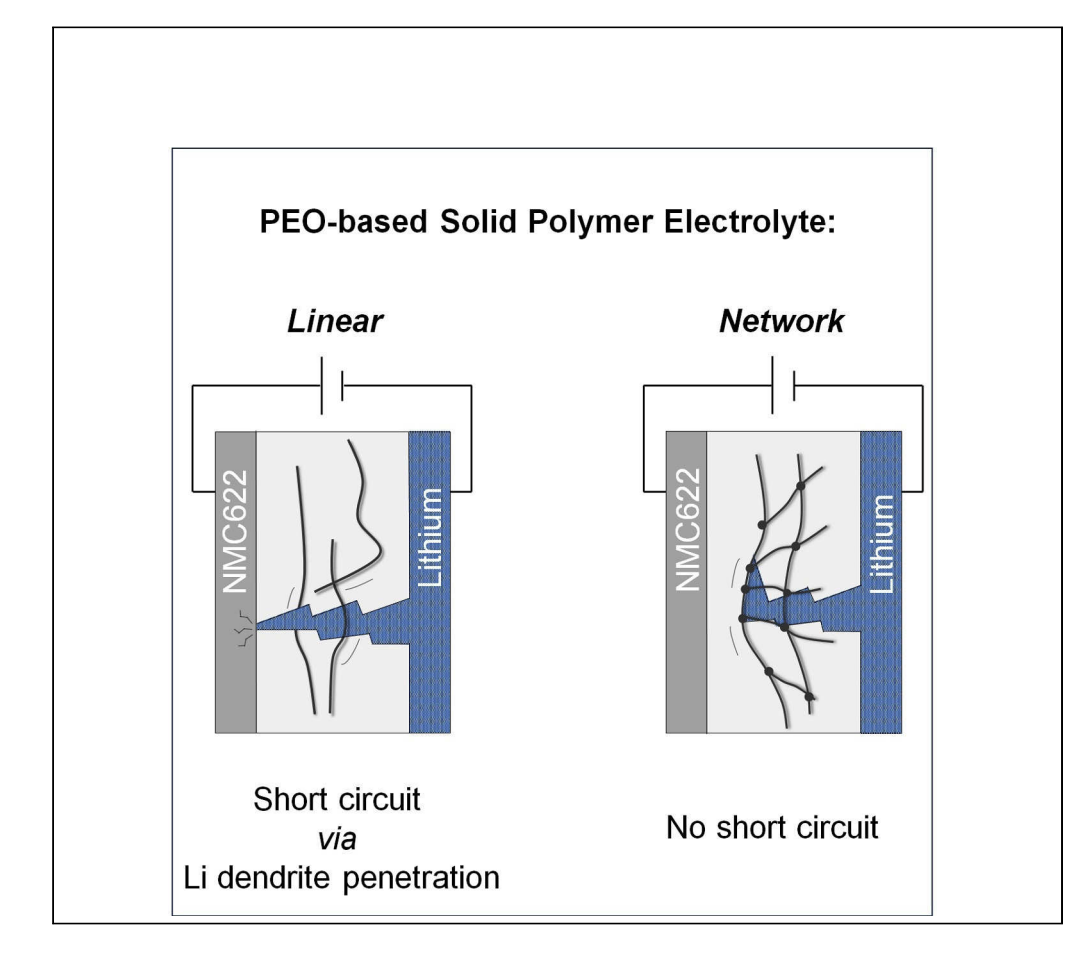
iScience



Article

Elimination of "Voltage Noise" of Poly (Ethylene Oxide)-Based Solid Electrolytes in High-Voltage Lithium Batteries: Linear versus Network Polymers



Gerrit Homann, Lukas Stolz, Martin Winter, Johannes Kasnatscheew

m.winter@fz-juelich.de (M.W.) j.kasnatscheew@fz-juelich.de (TK)

HIGHLIGHTS

PEO-based solid polymer electrolytes (SPEs) are stable up to 4.6 V versus Li|Li⁺

But, *linear* PEO-based SPE results in a "voltage noise-failure" in NMC||Li cells

Failure disappears when PEO is incorporated in a semi-interpenetrating network

Charge/discharge cycling possible even at 40°C in NMC622||Li cells

Homann et al., iScience 23, 101225 June 26, 2020 © 2020 The Author(s). https://doi.org/10.1016/ j.isci.2020.101225



iScience



Article

Elimination of "Voltage Noise" of Poly (Ethylene Oxide)-Based Solid Electrolytes in High-Voltage Lithium Batteries: Linear versus Network Polymers

Gerrit Homann, Lukas Stolz, Martin Winter, 1,2,* and Johannes Kasnatscheew 1,3,*

SUMMARY

Frequently, poly(ethylene oxide) (PEO)-based solid polymer electrolytes (SPEs) reveal a failure with high-voltage electrodes, e.g. LiNi $_{0.6}$ Mn $_{0.2}$ Co $_{0.2}$ O $_{2}$ in lithium metal batteries, which can be monitored as an arbitrary appearance of a "voltage noise" during charge and can be attributed to Li dendrite-induced cell micro short circuits. This failure behavior disappears when incorporating *linear* PEO-based SPE in a *semi-interpenetrating network* (*s-IPN*) and even enables an adequate charge/ discharge cycling performance at 40°C. An impact of any electrolyte oxidation reactions on the performance difference can be excluded, as both SPEs reveal similar (high) bulk oxidation onset potentials of \approx 4.6 V versus Li|Li $^+$. Instead, improved mechanical properties of the SPE, as revealed by compression tests, are assumed to be determining, as they mechanically better withstand Li dendrite penetration and better maintain the distance of the two electrodes, both rendering cell shorts less likely.

INTRODUCTION

Compared with a Li metal battery (LMB) with liquid electrolyte, an LMB with a solid electrolyte can improve safety, specific energy (e.g., via bipolar stacking), and cycle life, while still taking advantage of the high capacity of the Li metal electrode (Janek and Zeier, 2016; Jung et al., 2019; Schmuch et al., 2018; Betz et al., 2019). There are two classes, the inorganic- (e.g., glasses, ceramics) and organic-based solid electrolyte materials (e.g., polymers), each with characteristic pros and cons (Placke et al., 2017; Liang et al., 2018, 2019; Wang et al., 2020).

In general, inorganic electrolyte materials can reveal good ionic conductivities (e.g., $Li_{10}GeP_2S_{12}$ up to 10^{-2} S cm⁻¹ at 300 K) (Kwon et al., 2015; Culver et al., 2018; Mo et al., 2012), but in ceramic powdery form, their particle-based grain boundary resistances and low wettability with composite electrodes remain a challenge (Han et al., 2018; Xu et al., 2018). Hence, the superior wettability of solid polymer electrolytes (SPEs) renders them a better candidate (Seki et al., 2005) but, given their poor ionic conductivities (S cm⁻¹), only in thin layers (higher conductance [S]) (Janek and Zeier, 2016; Nair et al., 2019; Wu et al., 2019).

Typical polymer materials for SPEs are based on abundant and cheap *linear* poly (ethylene oxide) (PEO) (Nair et al., 2019; Snyder et al., 2007; Xu, 2004; Armand, 1994; Xue et al., 2015; Dias et al., 2000). Application with the common high-voltage/energy electrodes like LiNi_{0.6}Mn_{0.2}Co_{0.2}O₂ (NMC622), as a material with reasonable compromise with regard to specific capacity, specific energy, thermal/structural stability, and cycle life (Kasnatscheew et al., 2017a, 2017b, 2019), is challenging as during the charge process a "voltage noise" failure occurs, which is interpreted as cell micro-short circuits via penetrated Li dendrites (a morphology variation of high surface area lithium [Homann et al., 2020b; Bieker et al., 2015; Heine et al., 2015; Duan et al., 2018; Choudhury, 2018]) (Homann et al., 2020b). Therefore, a voltage noise-free cycling with the simple and conventional PEO-based SPE on high-voltage electrodes can only proceed for increased SPE thicknesses (e.g., multilayer approach) (Homann et al., 2020b; Wang et al., 2019), or with Li metal-free insertion-based negative electrodes, e.g., graphite, as shown in previous work (Homann et al., 2020b).

The key to circumvent this issue is consequently related with the suppression of Li dendrite penetration through the SPE. In this work a simple, economic, and effective strategy is introduced to mitigate the penetrability of the SPE, which is based on the formation of a *semi-interpenetrating network* (s-IPN) (Zeng et al., 2016), but in this

¹Helmholtz-Institute Münster, IEK-12, Forschungszentrum Jülich GmbH, Corrensstraße 46, 48149 Münster, Germany

²MEET Battery Research Center, Institute of Physical Chemistry, University of Münster, Corrensstraße 46, 48149 Münster, Germany

³Lead Contact

*Correspondence: m.winter@fz-juelich.de (M.W.), j.kasnatscheew@fz-juelich.de (J.K.)

https://doi.org/10.1016/j.isci. 2020.101225







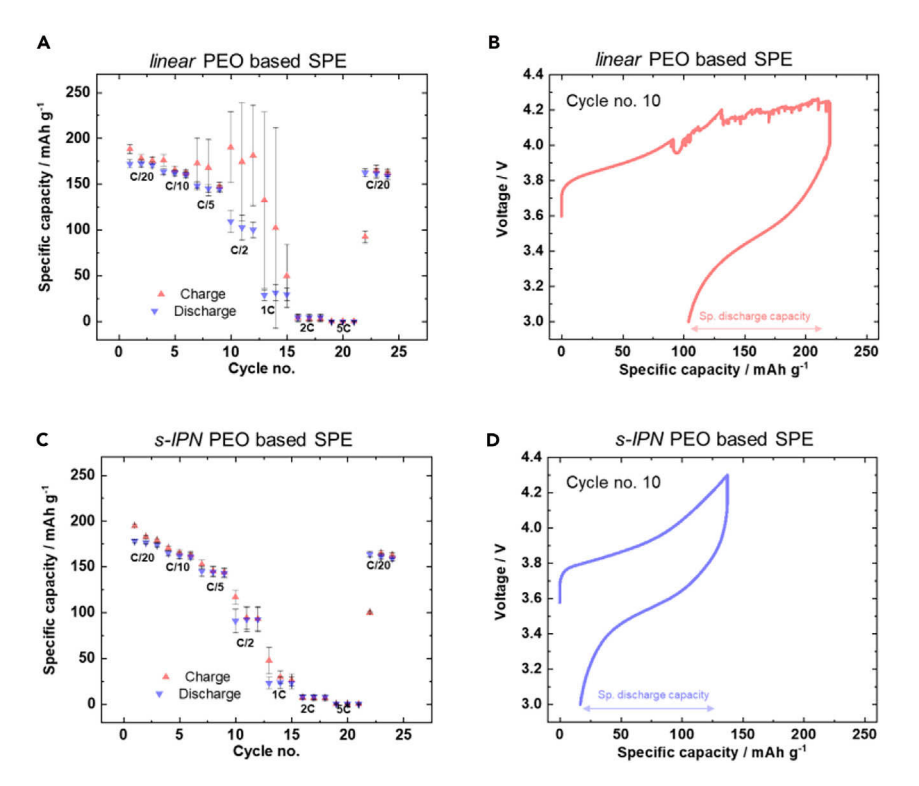


Figure 1. Galvanostatic Experiments of NMC622|SPE|Li Cells in the Voltage Range 4.3–3.0 V (Triple Determination) at 60° C. 1C Corresponds to a Specific Current of 150 mA g⁻¹

(A) C-rate examination using a linear PEO-based SPE. Cell failure is visible by increased specific charge capacities and deviations after a few cycles.

(B) Voltage curve of the 10th cycle (C/2) as an exemplary "failure" cycle with increased specific charge capacity showing a voltage noise as an arbitrary voltage increase/decrease leading to additional charge capacity.

(C) C-rate examination using an s-IPN PEO-based SPE. The cycles reveal similar discharge capacities as for the linear PEO-based SPE but without the severe increased and deviating specific charge capacities.

(D) Voltage curve of s-IPN PEO-based SPE of the exemplaric 10th cycle (C/2). The absence of voltage noise points to an improved ability of s-IPN PEO-based SPE to suppress Li dendrite penetration, without decay in specific discharge capacities.

work, mainly constituted from PEO units (Oh et al., 2003). On the basis of this strategy this work highlights the significant role of the mechanical electrolyte property as an important criterion to design SPEs for LMB enabling a voltage noise-free performance with high-voltage electrodes, even for thin (single-layer) SPEs.

RESULTS AND DISCUSSION

Higher current densities/C-rates facilitate Li dendrite growth and penetration (Gupta et al., 2018). To effectively investigate and screen the penetrability and the performance of each SPE with 100 μ m thickness, charge/discharge cycling with steadily increasing C-rates (C-rate test) is carried out for NMC622 | SPE | Li cells. As seen in Figure 1A, the specific charge capacities of *linear* PEO-based SPE start to significantly deviate for rates > C/5. This typical deviation of *linear* PEO-based SPE including higher specific charge capacities can be attributed to a process associated with a voltage noise during charge, as exemplarily shown in the voltage curves for 10^{th} cycle (C/2) in Figure 1B. The voltage noise as an arbitrary increase/decrease of voltage combined with the gained severe extra capacity during charge can be reasonably related to micro short circuits via penetrated Li dendrites through the SPE as shown in previous work (Homann et al., 2020b).

Given the simple one-pot reaction using cheap and abundant PEO with a network former (NF) (Scheme S1), the formation of an *s-IPN*-based SPE can be an effective and economic way to mitigate Li dendrite penetration. Indeed, for a content of NF above 45 wt % the described failure disappears as seen in Figure 1C. The accompanied nonappearance of voltage noise as exemplarily shown in voltage curve in Figure 1D for the 10th cycle (C/2) finally points to the absence of cell short circuits induced by Li dendrite penetration. The





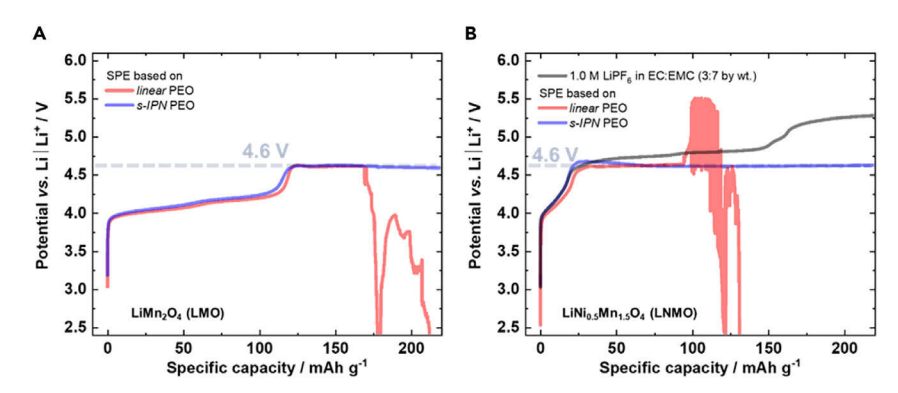


Figure 2. Anodic Stability Tests

Galvanostatic overcharge experiment to determine the bulk oxidation onset of the electrolytes using a specific current of 15 mA g^{-1} for validity reasons on (A) LMO and (B) LNMO electrodes. Independent of the used active material a potential plateau at $\approx 4.6 \, \text{V}$ versus Li|Li+ is observed for both SPEs. The bulk oxidation onset of linear PEO and s-IPN PEO-based SPEs is similar (high) and thus is unlikely to be the reason for the significant performance difference during C-rate tests as seen in Figure 1.

reversible specific capacities, i.e., specific discharge capacities remain similar for both SPEs. Thus, the elimination of voltage noise proceeds without obvious sacrifice in performance.

The significant difference of linear PEO and s-IPN PEO-based SPE, which interestingly is seen solely in the charge behavior, may be due to SPE oxidation (Kasnatscheew et al., 2016; Mindemark et al., 2018; Xu, 2004). Therefore, a possible difference of the SPE oxidation onset is checked for validity reasons on LiMn₂O₄ (LMO) and LiNi_{0.5}Mn_{1.5}O₄ (LNMO), thus on Ni-free and Ni-containing spinel materials. Spinel-based composite electrodes are known to be stable under overcharge conditions (Kasnatscheew et al., 2017c; Xu et al., 1999). As displayed in Figure 2A, the characteristic LMO delithiation (Xu et al., 1999; Kasnatscheew et al., 2013) is similar for both SPEs. After LMO delithiation, both SPEs reveal a potential plateau at ≈ 4.6 V versus Li|Li⁺, before the typical "noisy" potential response appears for linear PEO-based SPE. The potential plateau can be interpreted as bulk oxidation reaction for both SPEs. To exclude a possible impact of the catalytic activity of Ni on the oxidation reaction, these experiments are also performed on LNMO (Figure 2B). After an LNMO characteristic initial partial charge of ≈25 mAh g⁻¹ (Streipert et al., 2017; Kasnatscheew et al., 2018), again both SPEs reveal a potential plateau at ≈ 4.6 V versus Li|Li⁺, again before the appearance of noisy potential response for the linear PEO-based SPE. The instability of the SPEs above 4.6 V versus Li|Li⁺ prevents further LNMO delithiation as would occur, for example, for the more stable LiPF6 in mixed carbonate solvent-based liquid electrolyte, e.g., in ethylene carbonate (EC) and ethyl methyl carbonate (EMC) (Kasnatscheew et al., 2016, 2017c). As seen in Figure 2B, it enables the LNMO delithiation at the potential range between 4.7 and 4.9 versus Li|Li $^+$, before the electrolyte oxidatively decomposes at > 5.2 V versus Li|Li $^+$ (60°C). Overall, similar oxidative stabilities for both SPEs cannot explain their significant performance differences shown in the C-rate test (Figure 1).

The key for voltage noise-free performance during charge is obviously not electrochemically (thus electrode potential) reasoned but is likely associated with the Li dendrite penetrability of the SPEs as postulated in previous work (Homann et al., 2020b). As shown in previous work, it arbitrarily appears independent of the electrode potential/voltage, specific current (C-rate), or cycle number and thus is hard to reproduce (Homann et al., 2020b). In line with these findings, the Li dendrites could be even detected and visualized in Li|SPE|Li cells (Gupta et al., 2018). Contrary to separators soaked with liquid electrolytes, the porosity of compressed polymers cannot be crucial. Rather, the different penetrability of SPEs may be related to mechanical properties; thus, they may explain the difference in performance in Figure 1.

The compressibility of solid materials as a well-known mechanical property also in battery research and development can be used as reasonable criterion for the ability to withstand dendrite penetration (Galeski, 2003; Yan et al., 2018; Lehmann et al., 2019). As schematically shown in Figure 3A, the compressibility of a material can be measured between two plates with controlled decrease in their distance, thus with a steady increase in compressive strain (%), where 0% strain represents no shrinkage/thinning (initial distance between the plates) and 100% strain represents full shrinkage (zero distance between the plates,





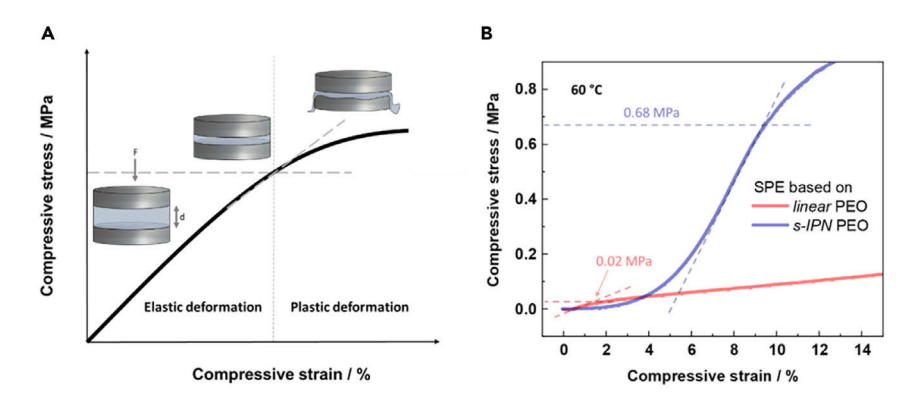


Figure 3. Mechanical Stability Tests

different electrochemical performance displayed in Figure 1.

(A) Schematic illustration of a compression test of a solid electrolyte. The compressive stress (F) is measured as a function of the compressive strain, which is induced by a steady decrease in distance (D) of the plates with the solid electrolyte in between, where 0% strain is regarded as the initial state and 100% strain is regarded as direct plate contact. The linear stress versus strain relation points to elastic (reversible) deformation, whereas the onset of curve flattening points to plastic (irreversible) deformation. The end of linearity indicates the stability limit of the electrolyte material.

(B) Compression curves of both SPEs at 60°C show a significantly higher limit for the s-IPN PEO-based SPE compared with linear PEO-based SPE with respect to compressive stress (\approx 0.68 versus \approx 0.02 MPa) and compressive strain (\approx 9.0% versus \approx 1.5%), demonstrating its mechanically more robust and elastic nature, respectively. This SPE can better withstand the stress originating from Li dendrite growth and shows more elasticity, thus maintaining the distance between the electrodes, which overall renders short circuits more difficult. This mechanical difference can explain the

i.e., both plates in contact). The required force for the applied strain increase is simultaneously measured and is named compressive stress (MPa).

A material possesses a reversible (elastic) compression nature when it is able to return to the initial state and shape after the end of applied compressive stress. As shown in Figure 3A, this elastic nature can be indicated via a linear relation between compressive stress and compressive strain. The subsequent onset of curve flattening is attributed to the onset of undesired irreversible (plastic) deformation, i.e., the material does not return to the initial state after the application of compressive strain is terminated. Consequently, the onset of plastic deformation can be regarded as material characteristic mechanical stability limit (Galeski, 2003; Yan et al., 2018; Lehmann et al., 2019). For example, for rather robust materials (e.g., ceramics) the compressive stress at the stability limit is rather high but typically comes with rather low compressive strain (indicating poor elastic behavior), whereas less rigid materials (e.g., some polymers) typically have the opposite characteristics (Galeski, 2003; Yan et al., 2018; Lehmann et al., 2019). In the ideal case, the solid electrolyte should have both robustness (e.g., for prevention of Li dendrite growth penetration) and elasticity (e.g., for better wettability and processability) (Janek and Zeier, 2016; Jung et al., 2019; Schmuch et al., 2018; Betz et al., 2019).

In Figure 3B, the compression features of each of the SPEs are investigated at battery cell operation conditions (60°C). With progressively increasing compressive strain (thus controlled decrease in plate distance), the *linear* PEO-based SPE starts to plastically deform already for a compressive strain of 1.5% at a compressive stress of only \approx 0.02 MPa. In contrast, no plastic deformation is detected for the *s-IPN* PEO-based SPE up to a compressive strain of 9% and a compressive stress of \approx 0.68 MPa. The higher compressive strain of the *s-IPN* PEO-based SPE demonstrates a significantly better elastic nature (e.g., the ability to mechanically better withstand volume changes), whereas the higher compressive stress demonstrates better ability to withstand external forces such as those coming from dendrites. This *mechanical* difference helps to explain the *electrochemical* performance difference in Figure 1: the *linear* PEO-based SPE easily relents to the pressure occurring from dendrite growth, which results in dendrite penetration, whereas the *s-IPN* PEO-based SPE can better withstand Li dendrite-induced stress and thus can better prevent the short circuit-associated voltage noise induced by Li dendrite penetration.

Based on the mechanical measurements it can be generally concluded that, compared with the *linear* PEO-based SPE not only more force is necessary for penetration through the s-IPN-based SPE but also more force is necessary for shrinkage/thinning of the s-IPN PEO-based SPE, thus for decreasing the

iScience Article



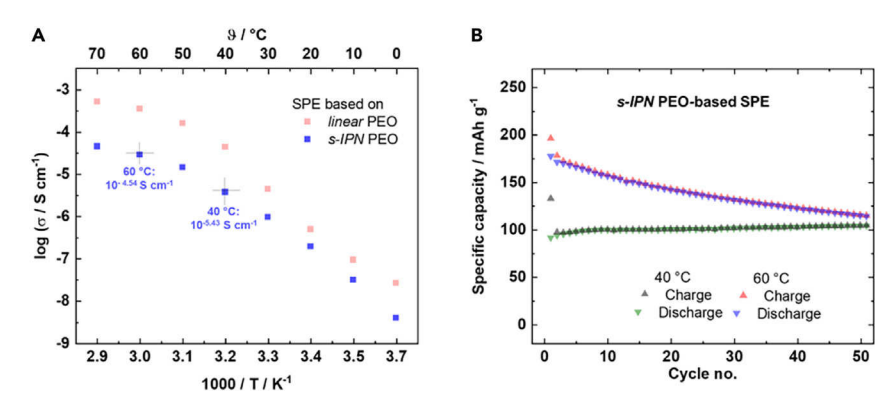


Figure 4. Electrochemical Performance

(A) Ionic conductivities of linear PEO and s-IPN PEO-based SPEs in the range of 70° C -0° C. The rigid nature of s-IPN-based SPE reveals a lower ionic conductivity compared with more flexible linear PEO-based SPE.

(B) Charge/discharge cycling performance of s-IPN-based SPE in an NMC622|SPE|Li cell (4.3–3.0 V, $0.1C = 15 \text{ mA g}^{-1}$). Despite lower ionic conductivity, the s-IPN-based SPE reveals high specific capacities at 60° C and even moderate specific capacities at 40° C with a high capacity retention over 50 charge/discharge cycles.

distance between the electrodes. Both are beneficial for LMB application as the risk of cell short circuits is reduced.

It has to be noted that the measurement reflects the mechanical properties of the sample at operation temperature of 60° C, whereas the sample preparation is performed at room temperature, where stability for both SPEs is significantly higher, that is ≈ 4 MPa for *linear* PEO-based SPE and even without plastic deformation for *s-IPN* PEO-based SPE in the detection limit up to 26 MPa.

The mechanically stable nature of the s-IPN PEO-based SPE reveals less "free volume" domains for segmental chain motions (Ratner and Shriver, 1988; Mindemark et al., 2018; Porcarelli et al., 2016), which results in lower ionic conductivity compared with *linear* PEO-based SPE as shown in Figure 4A. Although the ionic conductivity, e.g., at 40° C or at 60° C (Figure 4A), is lower for s-IPN- compared with that of *linear* PEO-based SPE, still good specific capacities are obtained for NMC622 (Homann et al., 2020a), as depicted in Figure 4B. Although the *linear* PEO-based SPE would end in an immediate voltage noise failure rendering the charge/discharge cycling hardly possible (Homann et al., 2020b), the s-IPN PEO-based SPE can cycle without the respective failure, e.g., without any deviations in specific charge capacities (cf. Figure 1). This points to the absence of voltage noise and detrimental short circuits, thus demonstrating a successful suppression of Li dendrite penetration during charge/discharge cycling. In this way a benchmark for a PEO-based SPE can be realized for R&D, which is hardly possible for PEO-based SPE in the conventional *linear* manner (Homann et al., 2020b). Interestingly, the rather low ionic conductivity of $10^{-5.43}$ S cm $^{-1}$ (0.004 mS cm $^{-1}$) at 40° C for the s-IPN PEO-based SPE is obviously sufficient to obtain moderate specific capacities (≈ 100 mAh g $^{-1}$) even with a high capacity retention.

Conclusion

In Li metal battery cells with high voltage/energy positive electrodes like LiNi $_{0.6}$ Mn $_{0.2}$ Co $_{0.2}$ O $_{2}$ (NMC622), the abundant and cheap *linear* poly(ethylene oxide) (PEO)-based solid polymer electrolyte (SPE) reveals a cell failure observable as voltage noise during charge. This failure disappears when modifying the *linear* PEO-based SPE to an *s-IPN* PEO-based SPE.

Electrochemical stability reasoned differences can be ruled out, because the main oxidation onset for both SPEs is similar as seen by potential plateaus at $\approx 4.6~\rm V$ versus Li|Li⁺ on LiMn₂O₄ (LMO) and LiNi_{0.5}Mn_{1.5}O₄ (LNMO) electrodes. Rather, mechanical properties associated with the Li dendrite penetrability of the SPEs from the Li electrode are more likely to cause the performance difference. It can be shown that *linear* PEO-based SPE can hardly withstand compression and plastically deforms already at a compressive stress of $\approx 0.02~\rm MPa$, whereas the s-*IPN* PEO-based SPE can withstand a compressive stress up to $\approx 0.68~\rm MPa$ at 60°C. Contrary to *linear* PEO-based SPE, the s-*IPN* PEO-based SPE can (1) mechanically more withstand Li dendrite growth through the SPE as well as (2) maintain the distance between the





electrodes during cell operation, thus rendering overall Li dendrite penetration and resulting short circuits less likely.

Despite a lower ionic conductivity due to the mechanically stable but rigid structure, thus allowing less chain mobility, the s-IPN PEO-based SPE reveals a specific capacity of \approx 100 mAh g $^{-1}$ and high capacity retention in an NMC622|SPE|Li cell at 40°C. It can be concluded that, despite the similar chemical composition of the two investigated SPEs, the key for voltage noise-free performance with high-voltage electrodes is related to suppression of Li dendrite penetrability through the SPE and can be significantly improved in a physical manner, in particular by designing the mechanical properties.

Limitations of the Study

The ionic conductivity of the solid polymer electrolyte can be further optimized by, e.g., Li salt concentration. Mass loading does not exceed 6 mg $\,\mathrm{cm}^{-2}$ and need to be extended in order to further increase the gravimetric and volumetric energy of the cell.

Resource Availability

Lead Contact

Further information and requests for resources and reagents should be directed to and will be fulfilled by the Lead Contact, Johannes Kasnatscheew (j.kasnatscheew@fz-juelich.de).

Materials Availability

Materials availability is given in Supplemental Information.

Data and Code Availability

The data that support the findings of this study are available from the corresponding author upon reasonable request.

METHODS

All methods can be found in the accompanying Transparent Methods supplemental file.

SUPPLEMENTAL INFORMATION

Supplemental Information can be found online at https://doi.org/10.1016/j.isci.2020.101225.

ACKNOWLEDGMENT

Financial support from the German Federal Ministry for Education and Research within the project FestBatt (grant number: 13XP0175A) is gratefully acknowledged.

AUTHOR CONTRIBUTIONS

G.H., J.K., and M.W. conceived the idea and co-wrote the manuscript. G.H. carried out the experiments. L.S. supported the experiments and graph design.

DECLARATION OF INTERESTS

The authors declare no competing interests.

Received: April 30, 2020 Revised: May 12, 2020 Accepted: May 28, 2020 Published: June 26, 2020

iScience

Article



REFERENCES

Armand, M. (1994). The history of polymer electrolytes. Solid State Ionics 69, 309–319.

Betz, J., Bieker, G., Meister, P., Placke, T., Winter, M., and Schmuch, R. (2019). Theoretical versus practical energy: a plea for more transparency in the energy calculation of different rechargeable battery systems. Adv. Energy Mater. 9, 1803170.

Bieker, G., Winter, M., and Bieker, P. (2015). Electrochemical in situ investigations of SEI and dendrite formation on the lithium metal anode. Phys. Chem. Chem. Phys. 17, 8670–8679.

Choudhury, S. (2018). The many shapes of lithium. Joule 2, 2201-2203.

Culver, S.P., Koerver, R., Krauskopf, T., and Zeier, W.G. (2018). Designing ionic conductors: the interplay between structural phenomena and interfaces in thiophosphate-based solid-state batteries. Chem. Mater. *30*, 4179–4192.

Dias, F.B., Plomp, L., and Veldhuis, J.B.J. (2000). Trends in polymer electrolytes for secondary lithium batteries. J. Power Sources 88, 169–191.

Duan, H., Yin, Y.-X., Shi, Y., Wang, P.-F., Zhang, X.-D., Yang, C.-P., Shi, J.-L., Wen, R., Guo, Y.-G., and Wan, L.-J. (2018). Dendrite-free Li-metal battery enabled by a thin asymmetric solid electrolyte with engineered layers. J. Am. Chem. Soc. *140*, 82–85.

Galeski, A. (2003). Strength and toughness of crystalline polymer systems. Prog. Polym. Sci. 28, 1643–1699.

Gupta, A., Kazyak, E., Craig, N., Christensen, J., Dasgupta, N.P., and Sakamoto, J. (2018). Evaluating the effects of temperature and pressure on Li/PEO-LiTFSI interfacial stability and kinetics. J. Electrochem. Soc. 165, A2801–A2806.

Han, F., Yue, J., Chen, C., Zhao, N., Fan, X., Ma, Z., Gao, T., Wang, F., Guo, X., and Wang, C. (2018). Interphase engineering enabled all-ceramic lithium battery. Joule *2*, 497–508.

Heine, J., Hilbig, P., Qi, X., Niehoff, P., Winter, M., and Bieker, P. (2015). Fluoroethylene carbonate as electrolyte additive in tetraethylene glycol dimethyl ether based electrolytes for application in lithium ion and lithium metal batteries.

J. Electrochem. Soc. 162, A1094–A1101.

Homann, G., Meister, P., Stolz, L., Brinkmann, J.P., Kulisch, J., Adermann, T., Winter, M., and Kasnatscheew, J. (2020a). High-voltage all-solid-state lithium battery with sulfide-based electrolyte: challenges for the construction of a bipolar multicell stack and how to overcome them. ACS Appl. Energy Mater. 3, 3162–3168.

Homann, G., Stolz, L., Nair, J., Laskovic, I.C., Winter, M., and Kasnatscheew, J. (2020b). Poly(Ethylene oxide)-based electrolyte for solid-state-lithium-batteries with high voltage positive electrodes: evaluating the role of electrolyte oxidation in rapid cell failure. Sci. Rep. 10, 4390.

Janek, J., and Zeier, W.G. (2016). A solid future for battery development. Nat. Energy 1, 16141.

Jung, K.N., Shin, H.S., Park, M.S., and Lee, J.W. (2019). Solid-state lithium batteries: bipolar

design, fabrication, and electrochemistry. Chemelectrochem *6*, 3842–3859.

Kasnatscheew, J., Evertz, M., Streipert, B., Wagner, R., Klopsch, R., Vortmann, B., Hahn, H., Nowak, S., Amereller, M., Gentschev, A.C., et al. (2016). The truth about the 1st cycle coulombic efficiency of LiNi_{1/3}Co_{1/3}Mn_{1/3}O₂ (NCM) cathodes. Phys. Chem. Chem. Phys. 18, 3956–3965.

Kasnatscheew, J., Evertz, M., Kloepsch, R., Streipert, B., Wagner, R., Cekic Laskovic, I., and Winter, M. (2017a). Learning from electrochemical data: simple evaluation and classification of LiMO₂-type-based positive electrodes for Li-ion batteries. Energy Technol. *5*, 1670–1679.

Kasnatscheew, J., Evertz, M., Streipert, B., Wagner, R., Nowak, S., Cekic Laskovic, I., and Winter, M. (2017b). Improving cycle life of layered lithium transition metal oxide (LiMO₂) based positive electrodes for Li ion batteries by smart selection of the electrochemical charge conditions. J. Power Sources 359, 458–467.

Kasnatscheew, J., Streipert, B., Röser, S., Wagner, R., Cekic Laskovic, I., and Winter, M. (2017c). Determining oxidative stability of battery electrolytes: validity of common electrochemical stability window (ESW) data and alternative strategies. Phys. Chem. Chem. Phys. 19, 16078–16086.

Kasnatscheew, J., Röser, S., Börner, M., and Winter, M. (2019). Do increased Ni contents in LiNi $_{\rm k}$ Mn $_{\rm y}$ Co $_{\rm 2}$ O $_{\rm 2}$ (NMC) electrodes decrease structural and thermal stability of Li ion batteries? A thorough look by consideration of the Li $^+$ extraction ratio. ACS Appl. Energy Mater. 2, 7733–7737.

Kasnatscheew, J., Schmitz, R.W., Wagner, R., Winter, M., and Schmitz, R. (2013). Fluoroethylene carbonate as an additive for y-butyrolactone based electrolytes. J. Electrochem. Soc. *160*, A1369–A1374.

Kasnatscheew, J., Wagner, R., Winter, M., and Cekic-Laskovic, I. (2018). Interfaces and materials in lithium ion batteries: challenges for theoretical electrochemistry. Top. Curr. Chem. *376*, 16.

Kwon, O., Hirayama, M., Suzuki, K., Kato, Y., Saito, T., Yonemura, M., Kamiyama, T., and Kanno, R. (2015). Synthesis, structure, and conduction mechanism of the lithium superionic conductor Li10+delta Ge1+delta P2-delta S12. J. Mater. Chem. A 3, 438–446.

Lehmann, M.L., Yang, G., Gilmer, D., Han, K.S., Self, E.C., Ruther, R.E., Ge, S., Li, B., Murugesan, V., Sokolov, A.P., et al. (2019). Tailored crosslinking of poly(ethylene oxide) enables mechanical robustness and improved sodium-ion conductivity. Energy Storage Mater. 21, 85–96.

Liang, J.-Y., Zeng, X.-X., Zhang, X.-D., Wang, P.-F., Ma, J.-Y., Yin, Y.-X., Wu, X.-W., Guo, Y.-G., and Wan, L.-J. (2018). Mitigating interfacial potential drop of cathode–solid electrolyte via ionic conductor layer to enhance interface dynamics for solid batteries. J. Am. Chem. Soc. 140, 6767–6770.

Liang, J.-Y., Zeng, X.-X., Zhang, X.-D., Zuo, T.-T., Yan, M., Yin, Y.-X., Shi, J.-L., Wu, X.-W., Guo, Y.-G., and Wan, L.-J. (2019). Engineering janus interfaces of ceramic electrolyte via distinct functional polymers for stable high-voltage Li-metal batteries. J. Am. Chem. Soc. 141, 9165–9169.

Mindemark, J., Lacey, M.J., Bowden, T., and Brandell, D. (2018). Beyond PEO-Alternative host materials for Li⁺-conducting solid polymer electrolytes. Prog. Polym. Sci. 81, 114–143.

Mo, Y., Ong, S.P., and Ceder, G. (2012). First principles study of the Li10GeP2S12 lithium super ionic conductor material. Chem. Mater. 24, 15–17.

Nair, J.R., Imholt, L., Brunklaus, G., and Winter, M. (2019). Lithium metal polymer electrolyte batteries: opportunities and challenges. Electrochem. Soc. Interfaces *28*, 55–61.

Oh, B., Hyung, Y.E., Vissers, D.R., and Amine, K. (2003). Accelerating rate calorimetry study on the thermal stability of interpenetrating network type poly(siloxane-g-ethylene oxide) polymer electrolyte. Electrochim. Acta 48, 2215–2220.

Placke, T., Kloepsch, R., Dühnen, S., and Winter, M. (2017). Lithium ion, lithium metal, and alternative rechargeable battery technologies: the odyssey for high energy density. J. Solid State Electrochem. 21, 1939–1964.

Porcarelli, L., Gerbaldi, C., Bella, F., and Nair, J.R. (2016). Super soft all-ethylene oxide polymer electrolyte for safe all-solid lithium batteries. Sci. Rep. 6, 19892.

Ratner, M.A., and Shriver, D.F. (1988). Ion-transport in solvent-free polymers. Chem. Rev. 88, 109–124.

Schmuch, R., Wagner, R., Hörpel, G., Placke, T., and Winter, M. (2018). Performance and cost of materials for lithium-based rechargeable automotive batteries. Nat. Energy *3*, 267–278.

Seki, S., Kobayashi, Y., Miyashiro, H., Mita, Y., and Iwahori, T. (2005). Fabrication of high-voltage, high-capacity all-solid-state lithium polymer secondary batteries by application of the polymer electrolyte/inorganic electrolyte composite concept. Chem. Mater. 17, 2041–2045.

Snyder, J.F., Carter, R.H., and Wetzel, E.D. (2007). Electrochemical and mechanical behavior in mechanically robust solid polymer electrolytes for use in multifunctional structural batteries. Chem. Mater. 19, 3793–3801.

Streipert, B., Röser, S., Kasnatscheew, J., JANßEN, P., Cao, X., Wagner, R., Cekic-Laskovic, I., and Winter, M. (2017). Influence of LiPF6 on the aluminum current collector dissolution in high voltage lithium ion batteries after long-term charge/discharge experiments. J. Electrochem. Soc. 164, A1474–A1479.

Wang, C., Wang, T., Wang, L., Hu, Z., Cui, Z., Li, J., Dong, S., Zhou, X., and Cui, G. (2019). Differentiated lithium salt design for multilayered PEO electrolyte enables a high-voltage solid-state lithium metal battery. Adv. Sci. 6, 1901036.

Wang, Q., Cui, Z., Zhou, Q., Shangguan, X., Du, X., Dong, S., Qiao, L., Huang, S., Liu, X., Tang, K., et al. (2020). A supramolecular interaction strategy enabling high-performance all solid





state electrolyte of lithium metal batteries. Energy Storage Mater. 25, 756–763.

Wu, J., Rao, Z., Cheng, Z., Yuan, L., Li, Z., and Huang, Y. (2019). Ultrathin, flexible polymer electrolyte for cost-effective fabrication of all-solid-state lithium metal batteries. Adv. Energy Mater. *9*, 1902767.

Xu, K. (2004). Nonaqueous liquid electrolytes for lithium-based rechargeable batteries. Chem. Rev. 104, 4303–4417.

Xu, K., Ding, S.P., and Jow, T.R. (1999). Toward reliable values of electrochemical stability limits for electrolytes. J. Electrochem. Soc. 146, 4172–4178.

Xu, L., Tang, S., Cheng, Y., Wang, K., Liang, J., Liu, C., Cao, Y.-C., Wei, F., and Mai, L. (2018). Interfaces in solid-state lithium batteries. Joule *2*, 1991–2015.

Xue, Z.G., He, D., and Xie, X.L. (2015). Poly(ethylene oxide)-based electrolytes for lithium-ion batteries. J. Mater. Chem. A 3, 19218–19253.

Yan, S., Huang, X., and Xiao, X. (2018). Measurement of the through thickness compression of a battery separator. J. Power Sources 382, 13–21.

Zeng, X.-X., Yin, Y.-X., Li, N.-W., Du, W.-C., Guo, Y.-G., and Wan, L.-J. (2016). Reshaping lithium plating/stripping behavior via bifunctional polymer electrolyte for room-temperature solid Li metal batteries. J. Am. Chem. Soc. 138, 15825–15828.

Supplemental Information

Elimination of "Voltage Noise"

of Poly (Ethylene Oxide)-Based Solid Electrolytes

in High-Voltage Lithium Batteries: Linear versus Network Polymers

Gerrit Homann, Lukas Stolz, Martin Winter, and Johannes Kasnatscheew

Methods

a) Materials

Poly(ethylene oxide) (PEO, M_w 300.000 Da), 1-methyl-2-pyrrolidinone (NMP, anhydrous, 99.5%), and poly(ethylene glycol)dimethacrylate (PEGdMA, M_w 750 Da) were purchased from Sigma-Aldrich. Lithium bis(trifluoromethanesulfonyl)imide (LiTFSI, 99.9%) and polyvinylidene difluoride (PVdF, Solef 5130) were purchased from Solvay, France. Super C65 carbon black was received from Imerys, France. Mylar foil (100 μm thickness) was purchased from DuPont, USA. Battery grade electrolyte, 1 M LiPF₆ in a mixture of ethylene carbonate and ethyl methyl carbonate (EC/EMC 3:7 by wt.) (LP57 Selectilyte™) from BASF, was used as benchmark liquid electrolyte. The active materials LiNi_{0.6}Mn_{0.2}Co_{0.2}O₂ (NMC 622), LiNi_{0.5}Mn_{1.5}O₄ (LNMO), LiMn₂O₄ (LMO) and LiFePO₄ (LFP) were purchased from Targray, Canada. Lithium metal (Albermale) was used as counter and reference electrode. Material storage and sample preparations was performed in a dryroom (dew point -65°C). PEO was dried under vacuum (10⁻⁷ mbar) at 45°C and LiTFSI at 110 °C for 2 days before use. All other chemicals were used as received.

b) Linear PEO-based SPE membrane preparation

Linear PEO-based SPE polymer membranes were prepared by mixing of PEO (1 g) and LiTFSI (0.434 g)in in acetonitrile (6 g) using an EO:Li ratio of 15:1. The solvent was evaporated and the sample dried at 60 °C under reduced pressure (10^{-3} mbar). The resulting gum-like material was sandwiched between Mylar foil sheets and pressed at 100 °C with an applied pressure of 15 bar for 10 min. The thickness of the resulting membrane in the range of 100±5 µm was controlled by usage of a spacer.

c) s-IPN PEO-based SPE membrane preparation

The *s-IPN* PEO-based SPE was prepared by dissolving PEO (1 g), LiTFSI (0.568 g), PEGdMA (0.450 g, 45wt%) and Azobisisobutyronitrile (AIBN) (0.041 g, 2wt%) in acetonitrile (6 g) using an EO:Li ratio of 15:1. After homogenization the solution is casted on mylar foil and the solvent is evaporated. The membrane is polymerized under N_2 flux at 80 °C for 1 h and dried over night at 80 °C under reduced pressure (10⁻³ mbar). The concentration of PEGdMA is referred to the PEO content.

d) Electrode preparation and cell assembly

NMC622 electrodes consisting of 91wt% NMC622, 4wt% Carbon Black and 5wt% PVdF were prepared by dissolving PVdF in NMP followed by the addition of carbon black and NMC622. The mixture was homogenized using a dissolver. The slurry was casted on aluminium foil using a doctor blade with a wet coating thickness of 50 μm. The electrode sheets were dried for 3 hours at 80 °C under vacuum, punched into circular electrode and dried again over night at 120 °C before use. The average active mass loading of NMC622 electrodes was 4.1 mg cm⁻². For the LNMO electrodes 84wt% LNMO, 8wt% Carbon Black and 8wt% PVdF were used. For the LMO electrodes 80wt% LMO, 10wt% Carbon Black and 10wt% PVdF were used. The LNMO and LMO electrodes were prepared using the procedure described above. The average active mass loading was 6.3 mg cm⁻² and 3.2 mg cm⁻², respectively. All cells used in galvanostatic cycling tests were prepared in two electrode setup (coin cell) using the above mentioned

positive electrodes as working electrode, the PEO-based or s-IPN PEO-based SPE as polymer membrane (both 100 μ m) and lithium metal as negative electrode. Cells used for the determination of the oxidative stability were prepared in three-electrode setup using the above mentioned positive electrodes as working electrode, and lithium metal as counter and reference electrode.(Nölle et al., 2019)

e) Electrochemical measurements

All constant current cycling experiments were conducted on a Maccor Series 4000 battery cell test system at 60 °C (respectively 40 °C) in a climate chamber (Binder KB400). The used C-Rates and corresponding specific currents are mentioned within the text and/or in the figure captions.

f) Mechanical measurements

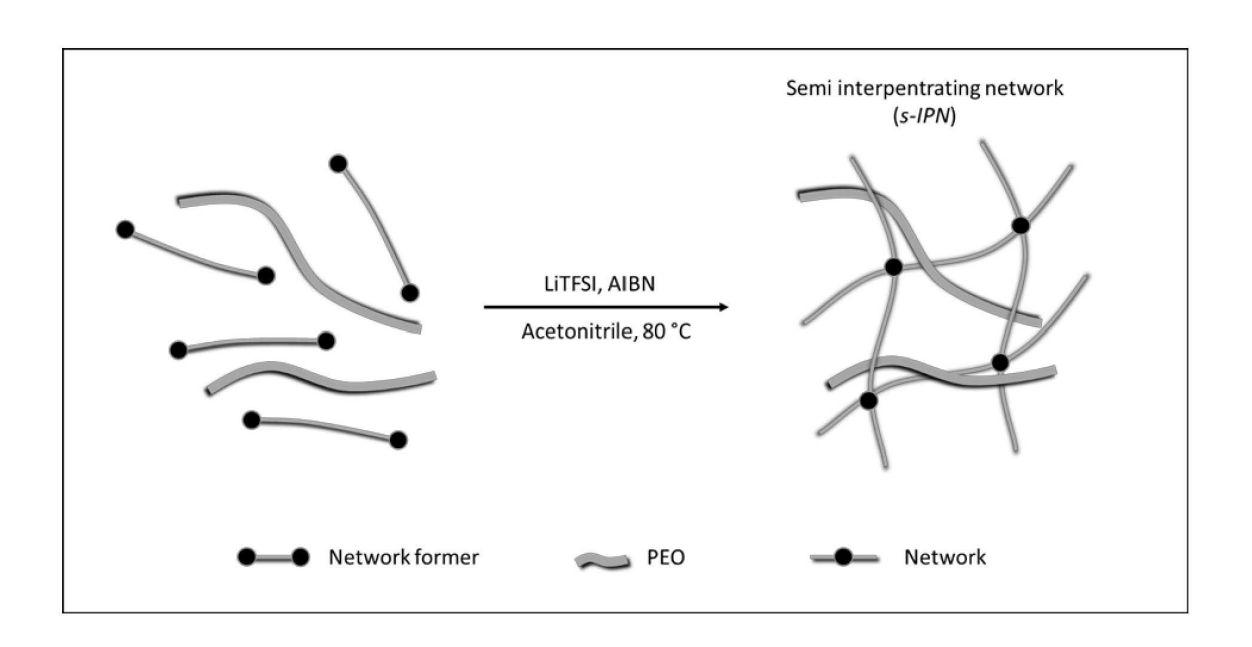
The compression behavior of the prepared SPE membranes was investigated using an Instron 5965 dual column universal testing machine (Instron, USA) with 50 mm compression plates. The samples were prepared by punching 18 mm discs of the SPE membranes with a thickness of approximately 2 mm. The measurements were performed with a speed of 20 $\mu m \ min^{-1}$ at 20 °C.

g) Ionic conductivity measurements

The electrochemical impedance spectroscopy (EIS) was conducted utilizing an Autolab PGSTAT302N with FRA32M high frequency analyser and MUX.SCNR16 16-fold multiplexer. The prepared SPE samples were sandwiched between stainless steel (SS) blocking electrodes and a PTFE spacer disc was used to keep the sample dimensions of 100 μ m height and 12 mm diameter constant in the coin cell (CR2032) housing. The sample cells were preheated at 70 °C for 2 h prior to the measurement to improve the surface wetting of the SS electrodes with the considered polymer samples. The EIS measurements were performed in the frequency range of 1 MHz to 1 Hz with an applied voltage amplitude of 10 mV in the temperature range of 0 °C to 80 °C in 5 °C steps. The temperature was controlled using a Binder MK53 climate chamber.

Supplemental reference

NÖLLE, R., BELTROP, K., HOLTSTIEGE, F., KASNATSCHEEW, J., PLACKE, T. & WINTER, M. 2019. A Reality Check and Tutorial on Electrochemical Characterization of Battery Cell Materials: How to Choose the Appropriate Cell Setup. *Materials Today*.



Scheme 1: Related to Figure 1. Synthesis route of the s-IPN PEO--based SPE. s-IPN can be regarded as trapped PEO chais in a polymerized network obtained via polymerization of network former based on poly(ethelene glycol)diemethacrylate (PEGdMA).